Available online at www.sciencedirect.com
SCIENCE DIRECT®
Carbohydrate Research 340 (2005) 835–839
Carbohydrate RESEARCH

Polysaccharide structures from powder diffraction data: molecular models of arabinan

Srinivas Janaswamy and Rengaswami Chandrasekaran*

Whistler Center for Carbohydrate Research, Department of Food Science, Purdue University, West Lafayette, IN 47907-2009, USA

Received 22 September 2004; accepted 16 December 2004

Dedicated to Professor David A. Brant

Abstract—X-ray intensity data from a polycrystalline sample of debranched arabinan, [→5)-α-L-Ara$_f$-(1→]$_n$, have been obtained using a powder diffractometer in order to determine its three-dimensional structure. The observed peaks index on a monoclinic cell with a = 5.444(7), b = 6.395(10), c = 8.680(5) Å, and γ = 99.6(3)°, V = 298 Å^3. One 2-fold helix along the c-axis can be accommodated in the unit cell. Molecular and packing models have been analyzed using the seven C-2′-*endo*/C-3′-*endo* allomorphs originally proposed by Radha and Chandrasekaran [*Carbohydr. Res.* **1997**, *298*, 105]. The generated powder pattern matches closely with the observed diffraction only for one C-2′-*endo* model. In this structure, the three main chain conformation angles are in the *trans* domains, there are no intra-chain hydrogen bonds, and the packing arrangement is stabilized by inter-chain O-3–H···O-2 bonds.

Keywords: Arabinan; Plant polysaccharide; Powder X-ray diffraction; Rietveld technique; Conformational analysis

1. Introduction

X-ray fiber diffraction is a powerful technique for unraveling polysaccharide structures. This experimental tool, combined with computer modeling, is instrumental in providing the molecular details and hence insights on several helix-forming biopolymers of biological and industrial importance. Unlike globular molecules that can produce single crystals, polysaccharides grow more readily along their helical axis, but to a limited extent in the basal plane. Under these circumstances, the best experimental specimen that could be produced is polycrystalline in which the individual crystallites are preferentially oriented along the helix axis. Thus, the resulting fiber diffraction pattern contains far fewer Bragg reflections than from single crystals. However, the important characteristics of the polysaccharide, namely the helical repeat and symmetry, along with the unit-cell dimensions, can be obtained accurately. Upon completion of a structure analysis using these intensity data, not only the molecular shapes but also intra- and inter-molecular contacts, hydrogen bonds, and interactions with counter-ions and solvent molecules that are otherwise responsible for structural stability and functional properties become fairly well defined. To date, the knowledge about the structure–function relationships of polysaccharides has relied mostly on their fiber patterns.[1,2] However, some biopolymers are not able to produce good quality fiber patterns, despite careful sample preparation by manipulating polymer concentration, pH, amount of salt, and temperature, and lead only to powder diffraction patterns. Two known examples are the debranched arabinan (derived from the plant polysaccharide arabinan),[3] and the branched bacterial polysaccharide S-657 in the gellan family.[4] The patterns are diagnostic of randomly oriented micro-crystals that fail to favor any specific alignment along the helix axis. In recent years, ab initio methods, combined with the Rietveld analysis (whole pattern profile fitting), have proven successful for solving inorganic as well as organic small-molecule structures from their powder intensity data.[5–7] To our knowledge,

* Corresponding author. Tel.: +1 765 494 4923; fax: +1 765 494 7953; e-mail: chandra@purdue.edu

0008-6215/$ - see front matter © 2005 Elsevier Ltd. All rights reserved.
doi:10.1016/j.carres.2004.12.035

polysaccharide structures have not been determined primarily from powder patterns except in one case, wherein electron-diffraction data from two-dimensional crystals combined with the profile intensities from powder samples have been utilized for elucidating the A-starch structure.[8] We are now adapting quantitative powder diffraction analysis as an auxiliary tool to identify the correct structure. We chose debranched arabinan (henceforth referred simply as arabinan for brevity) as the first test case for solving the three-dimensional structure from its powder intensities.

Native arabinan is a low molecular weight (6000–10,000 Da) plant polysaccharide component that is covalently linked to rhamnosyl residues in the rhamnogalacturonan region (so called 'hairy regions') of pectic polysaccharides. Those from beet, seeds, fruit, and roots are rich in arabinan. It is released from the pectic complex by alkaline treatment at elevated temperatures and is highly soluble. Its backbone is composed of a linear chain of (1→5)-linked α-L-arabinofuranosyl residues that is occasionally substituted at O-2 and/or O-3 with single α-L-arabinofuranosyl units.[9–12] Debranched arabinan, produced by controlled hydrolysis of native arabinan with α-L-arabinofuranosidase to remove essentially all of the O-2 and O-3 linked arabinofuranosyl units, could possibly be a good fat substitute, as its rheological properties closely mimic those of high-fat products. Also, its resistance to human digestive enzymes offers a potential usage in the food industry as a low-fat product.[11] It has been further used in cosmetics, pharmaceuticals, and toiletries.[12]

More than two decades ago, Churms et al.[13] reported a polycrystalline X-ray pattern for arabinan extracted from apple juice. Subsequently, molecular dynamics and NMR analysis by Cros et al. suggested six possible helical models (2, 3, 4, and 6-fold) with axial rise (h) per monomer unit ranging from 2.2 to 4.8 Å, incorporating either C-2′-*endo* or C-3′-*endo* sugar puckering as well as left- or right-handed chirality.[14] In the same year, a 2-fold helix of $h = 4.37$ Å was proposed by Chandrasekaran et al. based on conformational analysis and preliminary X-ray diffraction.[15] Later, energy calculations confirmed the 2-fold molecular structure and led to seven possible crystal-packing arrangements (three with C-2′-*endo* and four with C-3′-*endo* sugar puckering).[3] Even though the energy differences among them explain the polymorphic behavior of arabinan in mimicking fat properties, the lack of precise structural information on the polysaccharide is rather perplexing. In the case of inorganic and organic polycrystalline compounds, Rietveld analysis[16,17] is being used successfully for analyzing their structures. We are now applying this method in conjunction with the Linked-Atom Least-Squares (LALS) program,[18] a convenient tool for solving polymer structures, for determining the arabinan morphology. Preliminary results are reported in this article.

2. Experimental

2.1. Intensity data

A sample of purified arabinan was provided by the British Sugar Technical Center, Norwich, UK in powder form (manufactured by Megazyme International Ireland Limited). The compound was packed in an aluminum holder and X-ray intensity data were collected at room temperature over the 2θ range 10–36° at intervals of 0.01° on a Philips PW3710 diffractometer interfaced to a personal computer equipped with Automated Powder Diffraction (APD) software. The time spent at each step was 5 s. The X-ray tube was operated at 40 kV and 25 mA and Ni-filtered CuKα radiation was used in the data collection. The pattern was analyzed with the APD software to estimate peak positions.

2.2. Model building and refinement

The LALS program[18] was used for generating the molecular models incorporating C-2′-*endo* and C-3′-*endo* conformations for the furanose rings and examining the most probable packing arrangement of the arabinan helices. The function minimized in the least squares is given by

$$\begin{aligned} \Omega &= \Sigma_{i=1}^{I} e_i \Delta\theta_i^2 + \Sigma_{j=1}^{J} k_j \Delta c_j^2 + \Sigma_{h=1}^{H} \lambda_h G_h \\ &= E + C + L. \end{aligned}$$

The term E retains the I varied conformation and bond angles to be in their standard domains, while C optimizes the model against the J nonbonded as well as hydrogen-bonding interactions, and L becomes zero when the H constraints on helix symmetry are fully satisfied. The parameters e_i and k_j are the weights associated with the observations in the first two summations, respectively.

2.3. Pattern generation

The Rietveld program DB9807[19] was used for generating the powder patterns. The necessary half-width parameters were obtained by fitting the Caglioti et al.[20] formula and the background intensity was set as 100 counts. A pseudo-Voigt profile function was employed, with 12 times the Full Width at Half Maximum (FWHM) as the base width of the profile. The atomic scattering factors were from the program itself.

3. Results and discussion

The diffractogram is shown in Figure 1. The intensity distribution is consistent with that of a typical polycrystalline specimen. However, the profiles are broader than

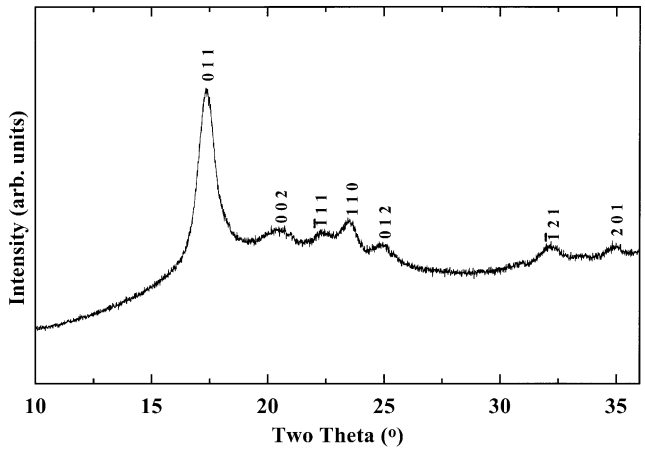

Figure 1. X-ray diffractogram of arabinan. The three integers at each peak top are the Miller indices. The pattern encompasses 29 independent Bragg reflections.

in inorganic compounds, suggesting that the crystallites are rather small in the sample. The APD program could identify seven significant peaks. The first at $2\theta = 17°$ is the strongest, and the remaining six are much less intense. Subsequently, these peaks could be indexed on a monoclinic unit cell with the DICVOL91[21] program in the Crysfire-suite.[22] The estimated figure of merit values were fairly high ($M_7 = 68.6$[23] and $F_7 = 36.8$[24]). Further refinement with the Celref program from the LMGP-suite[25] yielded the final unit-cell dimensions $a = 5.444(7)$, $b = 6.395(10)$, $c = 8.680(5)$ Å, and $\gamma = 99.6(3)°$. Table 1 lists the relative intensity, d-spacing, Miller indices, and observed and calculated Bragg angles for all these peaks.

Table 1. Relative intensity, d-spacing, Miller indices and observed and calculated Bragg angles in the diffractogram (Fig. 1) of arabinan [$a = 5.444(7)$, $b = 6.395(10)$, $c = 8.680(5)$ Å, and $\gamma = 99.6(3)°$]

Peak	Relative intensity	d (Å)	h	k	l	2θ(°)	
						Observed	Calculated
1	100.0	5.1055	0	1	1	17.355	17.361
2	7.8	4.3403	0	0	2	20.445	20.448
3	9.3	3.9736	−1	1	1	22.355	22.342
4	15.7	3.7849	1	1	0	23.485	23.476
5	6.9	3.5736	0	1	2	24.895	24.888
6	4.8	2.7861	−1	2	1	32.100	32.103
7	2.3	2.5644	2	0	1	34.960	34.967

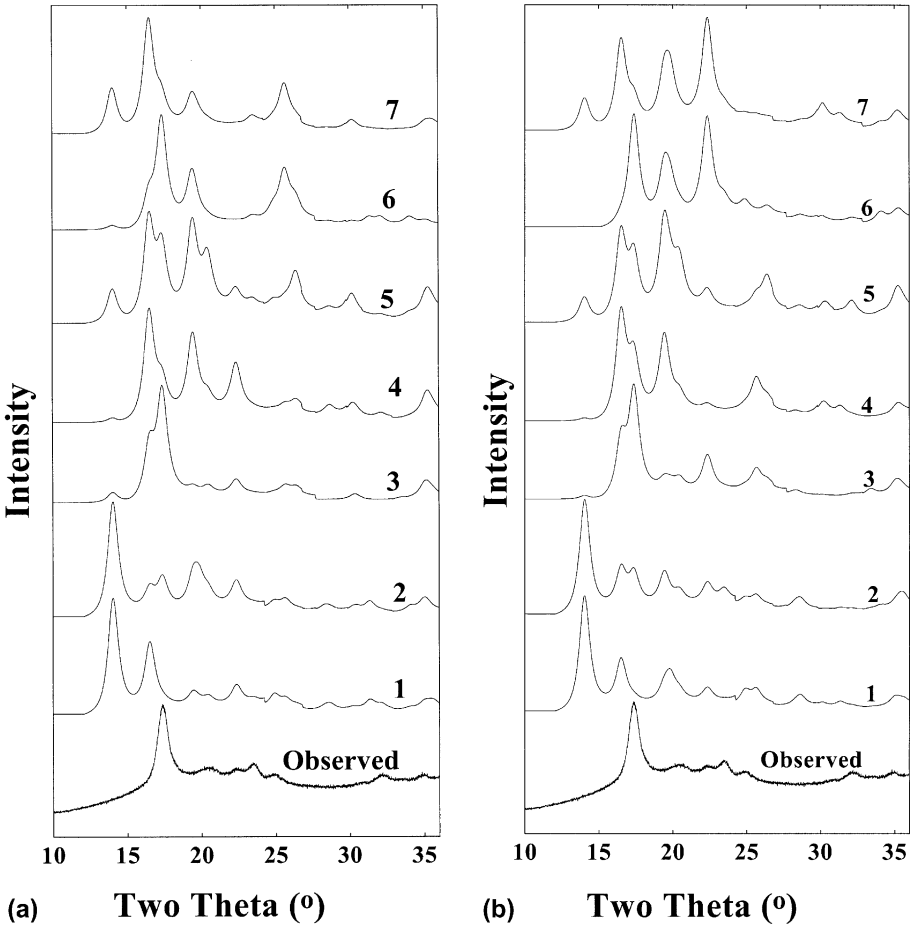

Figure 2. Comparison of the observed diffractogram with the generated powder patterns for the seven models **1**–**7**. The reducing ends of the helices are up-pointing in (a) and down-pointing in (b).

These unit-cell parameters are quite close to those previously reported: $a = 5.55$, $b = 6.14$, $c = 8.74$ Å, $\alpha = \beta = \gamma = 90°$.[3,15] Despite small changes in the individual values, the unit-cell volume remains unchanged at 298 Å^3. While it can easily accommodate two arabinosyl units, there is no room in the unit cell for any guest (water) molecules. Although hydrophilic biopolymers can bind water, arabinan without any water molecule behaves like a hydrophobic polymer in this polycrystalline state.

Among the seven 2-fold helical models of arabinan (labeled **1**–**7** in Table 2 of Ref. 3), **1**–**3** contain C-2′-*endo* and the rest C-3′-*endo* sugar puckering. The C-2′-*endo* models do not favor the *gauche plus* domain for ω (O-5–C-5–C-4–C-3). Depending on this and the other two conformation angles ϕ (C-2–C-1–O-5′–C-5′) and Ψ (C-1–O-5′–C-5′–C-4′), the packing energy values for these models were −1.1, −3.7, 2.3, −2.4, −2.8, −2.4, and −2.7 kcal/mol, respectively.[3] In the present work, these structures were used as the starting models for the LALS program[18] and the revised packing arrangements in the new unit cell (Table 1) were first examined by refining ω, ϕ, Ψ and the furanose ring geometry as well as the orientation μ (rotation about the *c*-axis) against intra- and inter-molecular nonbonded contacts. The atomic coordinates of each generated molecule were then adopted in the Rietveld program[19] to calculate its powder pattern. Figure 2a compares the diffraction profiles of the models, in which the reducing ends of the helices are up-pointing, with the observed pattern. While not present in the measured scan, an intense peak around $2\theta = 13°$ for models **1**, **2**, **5**, and **7** suggest that these arrangements are less favored in the sample. Similarly, due to a large profile around 20°, **4** and **6** are also ruled out. However, by providing a good match with the observed pattern except for some small intensity variations in the individual peaks, model **3** could possibly represent the arabinan structure. To check the influence

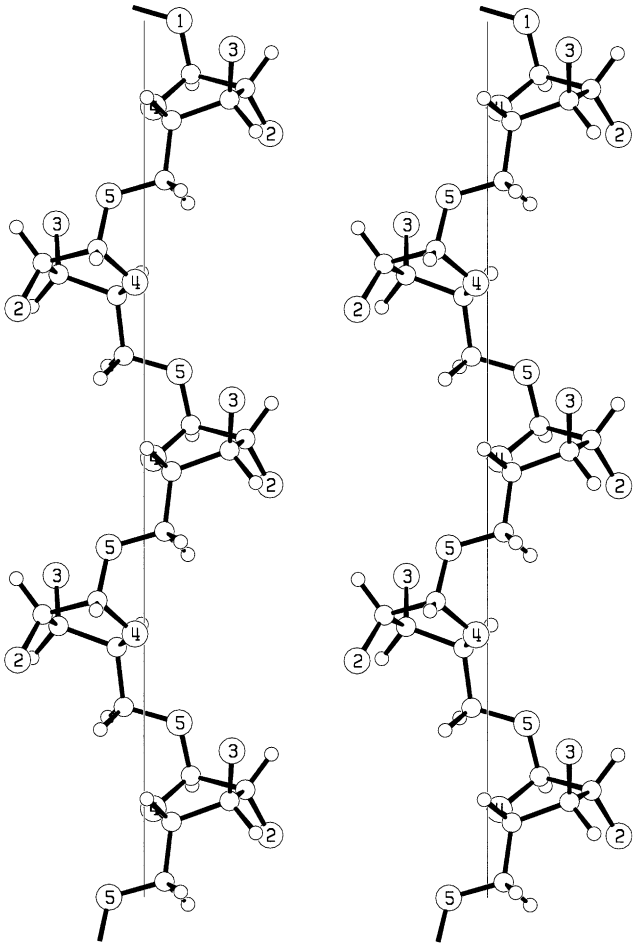

Figure 3. Stereo view of the arabinan helix. The sugar rings are approximately perpendicular to the helix-axis (vertical line).

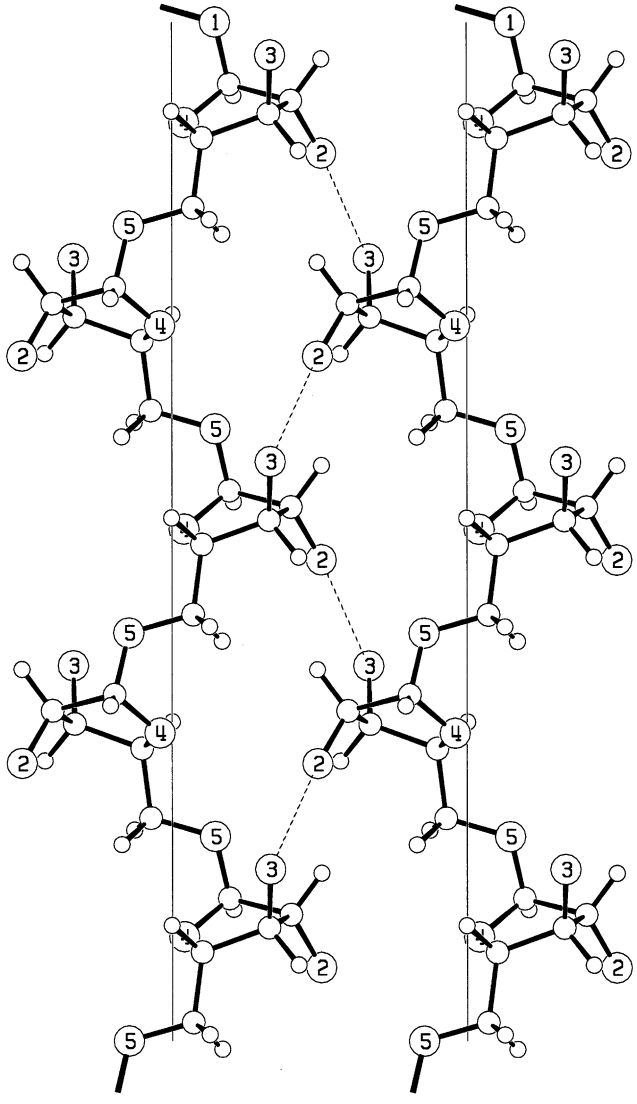

Figure 4. Association of helices, 6.1 Å apart, along the *b*-axis through inter-chain O-3–H···O-2 bonds. This will lead to a continuous stack of arabinan sheets separated by the cell edge *a*.

of absolute configuration, helix polarity was reversed in the unit cell and all of the foregoing calculations were repeated. The generated plots are presented in Figure 2b. Once again, model **3** is preferred over the rest. Thus, this analysis has narrowed down the seven models[3] to a single choice.

A stereo side view of the arabinan helix from model **3** is shown in Figure 3. In this structure, all the three angles (ω, ϕ, Ψ) are in the *trans* domain, 179°, −159°, and −174°, respectively. The C-2′-*endo* sugar rings are nearly perpendicular to the helix axis and there are no intra-chain hydrogen bonds to enhance chain rigidity. However, the packing of helices is mediated by inter-helical O-3-H···O-2 hydrogen bonds (Fig. 4) and van der Waals interactions.

4. Conclusions

Determination of polysaccharide architecture from powder X-ray intensities is the objective of the present analysis. In order to achieve this, three major points have to be considered: (1) identifying the correct unit-cell parameters, assignment of crystal symmetry and space group; (2) examining the possible molecular models; and (3) refining the structure against the X-ray intensities.

The first two have been addressed in this article. A new and better monoclinic unit cell (Table 1) has been identified from a high quality X-ray diffractogram (Fig. 1). The characteristics of the generated patterns for plausible crystal models point to model **3** as the most probable arabinan structure. However, all of these seven contenders have to be refined against the measured X-ray intensities so as to correctly determine the arabinan structure. This work is in progress.

Acknowledgements

This research was supported by the Industrial Consortium of the Whistler Center for Carbohydrate Research. We thank the referees for their helpful suggestions.

References

1. Chandrasekaran, R. *Adv. Carbohydr. Chem. Biochem.* **1997**, *52*, 311–439.
2. Chandrasekaran, R. *Adv. Food Nutr. Res.* **1998**, *42*, 131–210.
3. Radha, A.; Chandrasekaran, R. *Carbohydr. Res.* **1997**, *298*, 105–115.
4. Lee, E. J.; Chandrasekaran, R. *Carbohydr. Res.* **1991**, *214*, 11–24.
5. Poojary, D. M.; Clearfield, A. *Acc. Chem. Res.* **1997**, *30*, 414–422.
6. Porob, D. G.; Row, T. N. G. *Proc. Ind. Acad. Sci. Chem. Sci.* **2001**, *113*, 435–444.
7. Harris, K. D. M. *Curr. Opin. Solid St. M.* **2002**, *6*, 125–130.
8. Imberty, A.; Chanzy, H.; Perez, S.; Buleon, A.; Tran, V. *Macromolecules* **1987**, *20*, 2634–2636.
9. Thibault, J. F.; Guillon, F.; Rombouts, F. M. In *The Chemistry and Technology of Pectin Industry 6*; Phillips, G. O., Williams, P. A., Wedlock, D. J., Eds.; Academic: London, 1991; pp 119–133.
10. Kasapis, S.; Morris, E. R.; Norton, I. T. In *Gums and Stabilizers for the Food Industry 6*; Phillips, G. O., Williams, P. A., Wedlock, D. J., Eds.; IRL: Oxford, 1992; pp 419–428.
11. McCleary, B. V.; Cooper, J. M.; Williams, E. L. British Patent No. 8828378, 1989.
12. Cooper, J. M.; McCleary, B. V.; Morris, E. R.; Richardson, R. K.; Marrs, W. M.; Hart, R. J. In *Gums and Stabilisers for the Food Industry 6*; Phillips, G. O., Williams, P. A., Wedlock, D. J., Eds.; IRL: Oxford, 1992; pp 451–460.
13. Churms, S. C.; Merrifield, E. H.; Stephen, A. M.; Walwyn, D. R.; Polson, A.; Van der Merwe, K. J.; Spies, H. S. C.; Costa, N. *Carbohydr. Res.* **1983**, *113*, 339–344.
14. Cros, S.; Imberty, A.; Bouchemal, N.; Penkoat, C. H. D.; Pérez, S. *Biopolymers* **1994**, *34*, 1433–1437.
15. Chandrasekaran, R.; Radha, A.; Lee, E. J.; Zhang, M. *Carbohydr. Polym.* **1994**, *25*, 235–243.
16. Rietveld, H. M. *J. Appl. Crystallogr.* **1969**, *2*, 65–71.
17. Young, R. A. *The Rietveld Method*; Oxford University Press: IUCR, 1995.
18. Smith, P. J. C.; Arnott, S. *Acta Crystallogr.* **1978**, *A34*, 3–11.
19. Young, R. A. *J. Appl. Crystallogr.* **1995**, *28*, 366–367.
20. Caglioti, G.; Paoletti, A.; Ricci, F. P. *Nucl. Instrum. Methods* **1958**, *3*, 223–228.
21. Boultif, A.; Louer, D. *J. Appl. Crystallogr.* **1991**, *24*, 987–993.
22. Shirley, R. *The Crysfire 2002 System for Automatic Powder Indexing: User's Manual*; The Lattice: England, 2002.
23. Dewolff, P. M. *J. Appl. Crystallogr.* **1968**, *1*, 108–113.
24. Smith, G. S.; Snyder, R. L. *J. Appl. Crystallogr.* **1979**, *12*, 60–65.
25. Laugier, J.; Bochu, B. *LMGP-Suite Suite of Programs for the interpretation of X-ray Experiments*, http://www.inpg.fr/LMGP and http://www.ccp14.ac.uk/tutorial/lmgp/.